Epitranscriptomic profiling of VSMC phenotypes reveals uridine modifications linked to post-transcriptional regulation

Tobias Reinberger[1,2], Ayat Ismail[3], Torben Falk[1,2], Janina Fuß[4], Anja Wiechert[5,6], Elke Hammer[5,6], Tanja Zeller[1,2], Inken Wohlers[3,7,8,9*]

[1] Institute for Cardiogenetics, University Heart Center Lübeck, University Medical Center Schleswig-Holstein, Universität zu Lübeck, Germany

[2] DZHK (German Centre for Cardiovascular Research), Partner Site North, Germany; University Heart Centre Lübeck, 23562 Lübeck, Germany

[3] Biomolecular Data Science in Pneumology, Research Center Borstel, Leibniz Lung Center, Borstel, Germany

[4] Institute of Clinical Molecular Biology, Christian-Albrechts-University of Kiel, Kiel, Germany

[5] Department Functional Genomics, Interfaculty Institute of Genetics and Functional Genomics, University Medicine Greifswald, Greifswald, Germany

[6] DZHK (German Center for Cardiovascular Research), Greifswald, Germany

[7] University of Lübeck, Lübeck, Germany

[8] College of Medicine & Health Sciences, Khalifa University for Science and Technology, Abu Dhabi, United Arab Emirates

[9] Airway Research Center North (ARCN), German Center for Lung Research (DZL), Borstel, Germany

*Correspondence to iwohlers@fz-borstel.de, Research Center Borstel, Leibniz Lung Center, Parkallee 1, 23845 Borstel, Germany, +49 4537 / 188-6720

Keywords: Epitranscriptomics, RNA Modifications, Vascular Smooth Muscle Cells, Phenotypic Transition, Post-Transcriptional Regulation

Abstract

Background

Vascular smooth muscle cells (VSMCs) phenotypic plasticity can modulate atherosclerosis progression. Although several gene regulatory steps towards pro-inflammatory phenotypes have been well-studied, epitranscriptomic changes during this transition and their regulatory roles remain unexplored.

Methods and Results

Primary human VSMCs were stimulated with TGF-β1 to induce an atheroprotective, contractile, and matrix-producing state and with IL1-β plus PDGF-BB to induce a highly energetic, pro-inflammatory state, confirmed by Illumina bulk RNA sequencing and proteomics. Untargeted screening of mRNA base modifications using Oxford Nanopore Technologies direct RNA sequencing and xPore analysis revealed enhanced uridine modification within a GUUUU motif in pro-inflammatory VSMCs. Modified uridines were enriched in 3'-UTR and accessible RNA structures, with implications on Poly(A) tail dynamics and miRNA binding.

Conclusions

Atheroprotective and pro-atherogenic treatments induce distinct epitranscriptomic landscapes composed of different modification types, often co-localized in the same transcript. Modified uridines in mRNAs are abundant in a high-energy, pro-inflammatory VSMC state and associated with post-transcriptional regulation. In summary, epitranscriptomics adds a novel regulatory layer to VSMC phenotypic transitions critical for atherosclerosis development and progression.

Graphic Abstract

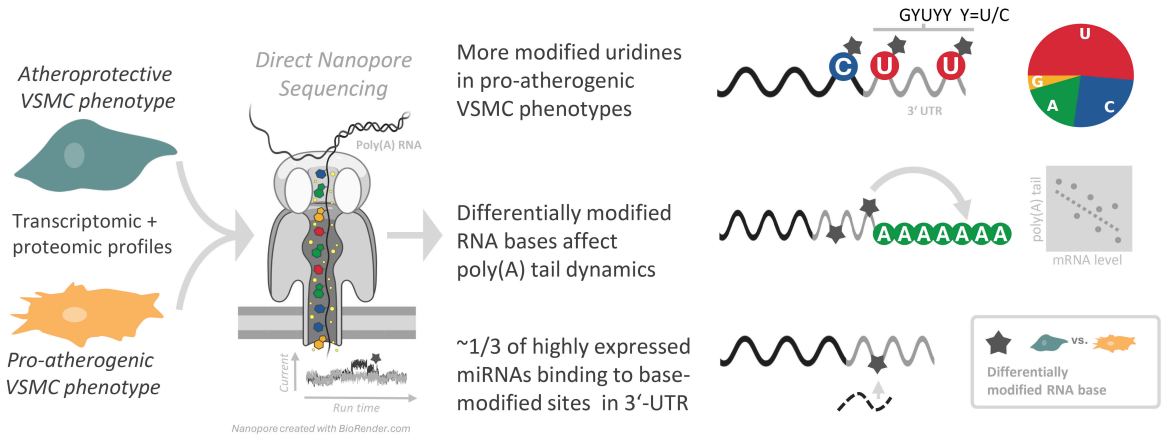

Introduction

Vascular cell adaptation within atherosclerotic plaques is one of the key features that modulate disease progression and can define the severity of atherosclerotic outcomes.[1] In particular, the immense plasticity of vascular smooth muscle cells (VSMCs) has been one of the research focuses in cardiovascular disease over the last years. While cytokine-driven pathways, key transcription factors, epigenetic mechanisms, and non-coding RNAs are well described to shape VSMC phenotypic transitions[2–5], the influence of epitranscriptomic regulation remains largely unexplored and is only beginning to receive attention.[6]

Epitranscriptomics characterizes and quantifies the collective set of chemical modifications of RNA. Previously, such modifications were investigated with techniques only dedicated to specific modification types, such as N6-methyladenosine (m^6A) and RNA types such as rRNA or tRNA.[7] With technological developments in third-generation sequencing, epitranscriptome-wide investigations are becoming feasible. Thereby, direct RNA sequencing of Oxford Nanopore Technologies (ONT) allows the hypothesis-free identification of modification sites by determining significant electric current differences between modified and unmodified bases, measured while RNA passes through a nanopore.[8]

More than 100 different types of RNA modifications have been described, and associations with many diseases have been reported.[9] Technology-fueled increased interest resulted in a few initial enzyme or modification-centered investigations in vascular disease published within the past five years.[10,11] The importance of epitranscriptomic regulation in VSMC phenotypic transitions is in the early stages of being recognized. For example, platelet-derived growth factor (PDGF)-BB-induced adenosines to inosines (A-to-I) editing has been described to foster the transition from the contractile, quiescent to a synthetic, pro-inflammatory VSMC state.[12] Furthermore, it has been demonstrated that m^6A mRNA methylation stabilizes transcripts of genes involved in VSMC-mediated vasoconstriction[13] and promotes VSMC proliferation, migration, and phenotypic switching[14], thereby highlighting the clinically relevant role of epitranscriptomic control in blood pressure and neointimal hyperplasia. Another disease-relevant RNA modification is 8-oxo-guanosine (8-oxoGuo), a product of RNA oxidation, which has been associated with atherosclerosis and reported as a predictor of mortality in individuals with type 2 diabetes.[15] Although the molecular consequences of RNA guanosine oxidation are well described in the context of cardiovascular diseases[16], the direct implication in VSMC biology remains elusive. Nevertheless, oxidative stress is widely accepted to play a key role in chronic inflammation, to contribute to VSMC phenotypic switching[17], and to promote the development of unstable plaques[18].

Here, we employed hypothesis-free ONT direct RNA sequencing to extend the spectrum of SMC-relevant RNA modifications beyond m^6A and to obtain an unbiased view of the global epitranscriptomic landscape across distinct VSMC phenotypic states. Inspired by a recent study in which ONT long-read cDNA sequencing has been applied to investigate alternative splicing of contractile and proliferative, pro-inflammatory phenotypes, represented by transforming growth factor β1 (TGF-β1)- and PDGF-BB-treated human aortic smooth muscle cells[19], we treated VSMCs with TGF-β1 to promote an atheroprotective state (later referred to as condition C3). This VSMC phenotype was compared to

102 pro-inflammatory/pro-atherogenic VSMCs under PDGF-BB / interleukin 1β (IL-1β)
103 treatment[20] (condition C4), and additionally to oxidative stress-prone VSMCs (C2) as well as
104 oxidatively stressed VSMCs (C1). Here, we demonstrate that epitranscriptomic alterations
105 drive post-transcriptional regulation by affecting mRNA processing, miRNA binding, and
106 translation, thereby determining VSMC states important for atherosclerotic disease
107 progression.
108

109 **Methods**

110 Key result files, scripts, and figures have been made publicly available at FAIRDOMHub
111 under "OMICS of vascular smooth muscle cells under oxidative stress" and can be accessed
112 at https://fairdomhub.org/projects/461. Transcriptome sequencing data (Illumina mRNA and
113 small RNA-Seq as well as ONT direct RNA-Seq) for this study have been deposited in the
114 European Nucleotide Archive (ENA) at EMBL-EBI under study accession number
115 PRJEB98980 (https://www.ebi.ac.uk/ena/browser/view/PRJEB98980). Proteomics raw data
116 files are available in PRIDE under accession ID PXD065513, currently accessible via
117 reviewer access token w5MHzwMvIHve. The modification workflow is available at
118 https://github.com/iwohlers/2025_ont_rnaseq_vsmc. A detailed method description,
119 Supplementary Figures, Supplementary Tables, and Major Resource Tables are available in
120 the Supplemental Material.
121

122 *Cell culture and functional assays of vascular smooth muscle cells*

123 Human primary vascular smooth muscle cells (VSMCs) were obtained from multiple
124 commercial vendors (Thermo Fisher Scientific/Gibco, Cell Applications, Inc., and
125 PromoCell), all of whom adhere to the principles of the Declaration of Helsinki (see
126 **Supplementary Table S1**). VSMCs were cultured and expanded up to passage eight. Since
127 VSMCs rapidly transform to a synthetic phenotype if seeded on a plastic surface, we
128 cultured VSMCs on a collagen I hydrogel instead. In brief, cells were seeded onto collagen I
129 hydrogels and allowed to attach for 24 h in medium containing 1% fetal bovine serum (FBS)

130 and 1 μM cytochalasin D to inhibit contraction, which was critical to ensure an even VSMC
131 monolayer for CellROX measurements. A contractile, atheroprotective phenotype was
132 induced by treatment with 5 ng/mL TGF-β1 and 1 μM cytochalasin D for four days, followed
133 by induction of a pro-inflammatory/ pro-atherogenic phenotype using 10 ng/mL PDGF-BB
134 and 10 ng/mL IL-1β for two days. Cells were subsequently used for CellROX assays and
135 RNA sequencing. Detailed culture conditions and hydrogel preparation are provided in the
136 Supplementary Material. A detailed description of functional assays such as oxidative stress
137 assays, quantification of the mitochondrial membrane potential and seahorse assays are
138 also provided in the Supplementary Material.

139

140 *Short-read RNA sequencing*

141 Short-read sequencing using the TrueSeq stranded mRNA library preparation kit was
142 performed for eight biological replicates (see **Suppl. Table S1**) and five conditions:
143 oxidatively-stressed VSMCs (C1; TGF-β1 and PDGF-BB / IL-1β + PDGF boost), oxidative
144 stress-prone VSMCs (C2; TGF-β1 and PDGF-BB / IL-1β), atheroprotective VSMCs (C3;
145 TGF-β1 only), proatherogenic VSMCs (C4; PDGF-BB / IL-1β only), and untreated VSMCs
146 (C5). RNA isolation and library preparation is descirped in the Supplementary Material. RNA
147 sequencing (RNA-Seq) datasets were analyzed using a community workflow from the
148 snakemake workflow catalog
149 (https://github.com/snakemake-workflows/rna-seq-kallisto-sleuth) version 2.8.4. A detailed
150 descrition of the workflow tools, which cover the enrichment analysis and isoform switch
151 analysis is provided in the in the Supplementary Material. Principal component analysis
152 (PCA) was performed for the 1,000 most variable genes after selecting the most highly
153 expressed transcript per gene and keeping only transcripts with a minimum normalized $\log_2$
154 expression of 6.

155

156 *Long-read direct RNA sequencing by Oxford Nanopore Technologies*

157 Stimulated VSMCs cultured on Col I hydrogels were subjected to direct RNA-Seq using
158 Oxford Nanopore Technologies (ONT) (**Suppl. Table S1**) und four the conditions C1 – C4
159 (see above). To trigger endogenous ROS production, VSMCs were incubated with 400
160 ng/mL PDGF-BB for 3 hours. RNA isolation was performed as described above for
161 short-read RNA-Seq. Approximately 10×10^6 stimulated cells per condition were used as
162 input for direct RNA-Seq. Library preparation and direct RNA-Seq were conducted according
163 to the ONT protocol SQK-RNA002. About 150 – 200 ng rRNA-depleted RNA was
164 sequenced for 18 - 22 hours uisng a GridION device with FLO-MIN106 flow cells with more
165 than 1000 active pores. ONT direct RNA-Seq data was processed using our own
166 snakemake workflow (in detailed described in the Supplementary Material and available at
167 https://github.com/iwohlers/2025_ont_rnaseq_vsmc), with tools installed in a reproducible
168 fashion via conda using environment files provided as part of the workflow. The workflow
169 uses guppy version 6.3.2 for basecalling and pycoQC[21] for quality control. Transcript
170 expression levels were determined using nanocount[21] (transcript annotation from Ensembl
171 v113). For differential modification detection, reads were mapped to transcript reference
172 sequences (Ensembl v113) using minimap2[22], followed by xPore[8] (version 2.1) used with
173 nanopolish eventalign output, *i.e.*, modification positions refer to transcript coordinates.
174 Poly(A) tail lengths were estimated using nanopolish mode 'polya' (coverage>10).
175 Coordinates of untranlasted regions (UTRs) and coding sequences (CDS) were obtained by
176 pybiomart v0.2.0. Normalization of nanocount counts and testing of differential expression
177 were performed with DESeq2[23], and an additional variance stabilization using rlog
178 transformation was performed before principal component analysis, both as previously
179 described for nanocount expression data.[21] These downstream analyses and visualizations
180 are available as part of the FAIRDOMHub under https://fairdomhub.org/projects/461.

181

Transcriptome-wide prediction of RNA structure elements

RNA secondary structure prediction and analysis were performed in Python using ViennaRNA and Forgi packages. For each modified base or k-mer, overlapping 150-nt mRNA sequence windows were extracted from Ensembl annotations and shifted stepwise across the modification site. Centroid secondary structures and minimum free energies (MFE) were predicted for each window. Structural similarity was quantified from dot–bracket representations using a sequence alignment–based scoring approach and used to cluster centroid structures by hierarchical clustering. Representative structures were selected based on cluster size and energy characteristics, and the lowest-MFE centroid structures were retained for downstream analysis. Secondary structure elements were annotated using Forgi, and enrichment of structural elements within k-mers was assessed using hypergeometric and Fisher's exact tests (for details see Supplementary Material).

Prediction of RNA structure elements with miRNA binding

Wide-window prediction (>350 nt) of RNA secondary structures was conducted with RNAplfold (version 2.7.0). Alignment of the miRNA involved two steps: local alignment of the seed sequence and global upstream alignment of the residual miRNA sequence (for details see Supplementary Material).

Small RNA sequencing

For the identification of highly expressed miRNAs, small RNA sequencing was performed for two technical replicates of four conditions (C2 – C5), respectively. Approximately 3.8×10^5 cells/well (HAOSMC IV) were seeded in 6-well plates that were covered with a Col I hydrogel (1.5 mg/mL). VSMCs were stimulated as described above for short-read RNA-Seq and RNA isolation, library preparation, and data analysis are described in the Supplementary Material. We investigated whether the modified base is part of miRNA seed regions, for which we considered 7mer-m8 sites, *i.e.*, bases 2-8 of the miRNA need to match

209 the reverse complement of the region covering the modified base. Seed regions were
210 obtained from Targetscan[24]. Annotation of publication-supported miRNA-target interactions
211 was obtained from MirTarBase[25].
212
213 *Proteomics*
214 Protein quantification in TGF-β1– and PDGF-BB–stimulated VSMCs was performed by
215 label-free quantitative mass spectrometry (MS) with four technical replicates per condition.
216 Proteins were extracted, quantified, enzymatically digested, and analyzed by
217 HPLC–ESI–MS/MS using an Orbitrap mass spectrometer. MS data were processed and
218 normalized with Spectronaut using a human UniProt reference database, and protein
219 abundances were calculated as maxLFQ values. Statistical analysis was performed at the
220 peptide level and protein set enrichment analysis was conducted using Enrichr[26]. Detailed
221 sample preparation, acquisition parameters, and analysis workflows are provided in the
222 Supplementary Material.
223
224 **Results**
225 *Energetic and transcriptomic profiling of VSMC phenotypes*
226 To study pro-atherogenic transitions of vascular smooth muscle cells with respect to
227 oxidative stress, inflammatory signaling, gene regulation, and epitranscriptomic changes, we
228 established an *in vitro* cell culture model and performed energetic and global transcriptomic
229 profiling of these VSMC phenotypes (**Figure 1A**, **Suppl. Figure S1A,** and **Suppl. Table S2**).
230 As previously described[27], activation of TGF-β signaling promoted a quiescent,
231 contractile-like VSMC phenotype, accompanied by reduced mitochondrial activity (**Suppl.**
232 **Figure S1**), higher level of canonical SMC contractile marker genes (*e.g. ACTA2*, *CNN1*,
233 *TAGLN*, and *LMOD1*; *cf.* **Suppl. Table S3**), and activation of genes involved in extracellular
234 matrix organization (ECM) (**Figure 1**). This mesenchymal-like, ECM-producing VSMC
235 phenotype can contribute to fibrous cap formation in atherosclerotic plaques[3] - a protective

236 layer that stabilizes fatty deposits in the vessel wall and helps prevent plaque rupture.
237 Therefore this VSMC phenotype is referred to as the atheroprotective VSMC state or C3
238 throughout the study.

239 PCA of the most variable expressed genes showed the largest variation (PC1) between
240 atheroprotective or untreated VSMCs (C3/C5) and PDGF-BB / IL-1β–treated VSMCs
241 (C1/C2/C4) (**Figure 1B, Suppl. Figure S2**). Of note, we added IL-1β as it can synergistically
242 promote PDGF signaling.[20] PDGF-BB / IL-1β–treated VSMCs (C4) exhibited an energetic
243 and pro-inflammatory signature, with enhanced mitochondrial and glycolytic activity as well
244 as increased expression of genes involved in cytokine-induced signaling (**Suppl. Figure S1**
245 **and Figure 1**). In particular IL-17, TNF/NF-κB, and RAS signaling pathways were shown to
246 worsen atherosclerosis and accelerate plaque progression.[28,29] Accordingly, PDGF-BB /
247 IL-1β–treated VSMCs (C4) are hereafter termed pro-atherogenic VSMCs.

248 In addition, we created an intermediate VSMC state (TGF-β1 > PDGF-BB / IL-1β; C2)
249 between atheroprotective and pro-atherogenic phenotypes, with mesenchymal
250 transition–associated genes remaining inactive (cluster 2) while extracellular matrix and
251 inflammatory genes are upregulated (clusters 1 and 6 in **Figure 1C**). Notably, impairment of
252 mesenchymal transition programs is often associated with reduced cellular adaptability to
253 stress.[30] Moreover, the concurrent production of ECM components and cytokines is
254 energy-demanding and is therefore associated with increased ROS levels, which can
255 promote mitochondrial dysfunction and overwhelm cellular antioxidant defenses. The
256 intermediate state is therefore termed oxidative stress–prone VSMCs.

257 Finally, we added very high levels of PDGF-BB to this oxidative stress–prone VMSC
258 phenotype characterized by elevated biosynthetic activity and reduced stress adaptation
259 capacity, since we suspected high local concentrations of PDGF in atherosclerotic lesions [31].
260 Indeed, hyperactivation of PDGF signaling resulted not only in elevated ROS levels (**Suppl.**
261 **Figure S1B**), most likely through activation of mitochondria and NADPH oxidase as
262 previously described[32], but also led to reduced expression of several genes essential for cell

function, accompanied by a strong upregulation of olfactory receptor genes (**Figure 1D**), which were found to regulate pathophysiological processes in SMCs and described as novel therapeutic targets.[33]

In addition to pronounced transcriptional changes (**Supplementary Fig. S3**), oxidative stress induced widespread differential splicing. A total of 1,298 genes exhibited significant splicing differences between atheroprotective VSMCs and pro-inflammatory phenotypes, with CCL20, CXCL8, FAH, and NOL4L consistently affected across all comparisons. For example, increased CCL20 expression in pro-atherogenic VSMCs was accompanied by preferential usage of isoforms containing the chemokine interleukin-8-like domain (**Suppl. Figure S4A**).

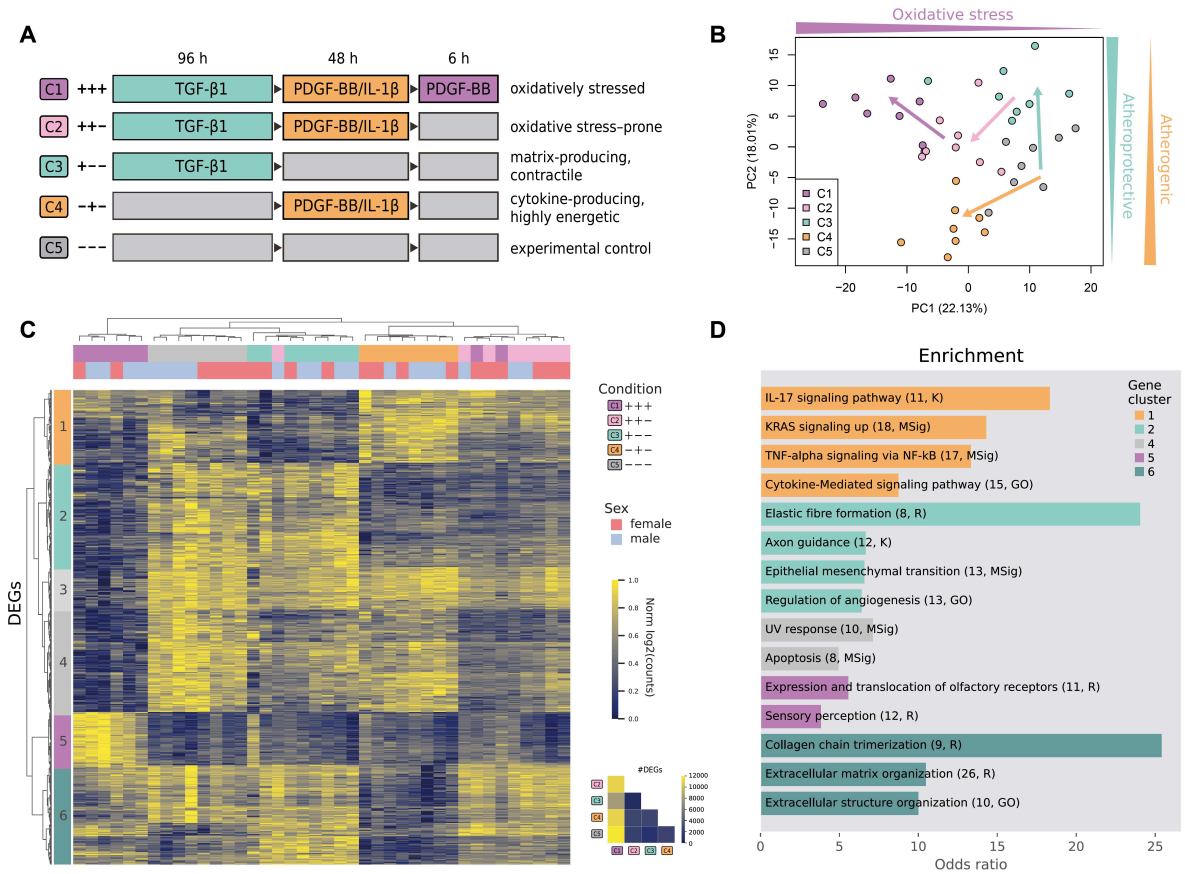

Figure 1: (**A**) Experimental design and definition of conditions C1–C5 used throughout the study. Each condition is sampled with eight biological replicates. (**B**) Principal component (PC) analysis of five conditions is based on the 1,000 most variable transcripts with normalized and batch-corrected $\log_2$ expression ≥ 5. (**C**) Clustered heatmap showing row-scaled expression of the 1,000 most variable canonical, differentially expressed transcripts (with FDR<=0.001; mean $\log_2$ count ≥ 5) from the joint model across all conditions. (**D**) Up to four top enriched

pathways for six gene clusters displaying condition-specific up- or down-regulation, colored according to the corresponding condition.

Epitranscriptomic profiling of VSMC phenotypes

In order to investigate whether pro-inflammatory conditions accompanied by high level of ROS can directly modulate mRNA base modifications, we used Oxford Nanopore (ONT) direct RNA sequencing and xPore to obtain a comprehensive overview of the RNA modification landscape. In general, up to 4% of mRNA bases of an individual transcript were found to be modified (*e.g.*, methylated; rate ≥ 0.5) in atheroprotective VSMCs (**Figure 2A** and **Suppl. Table S5**). While the absolute number of modified bases per transcript increases with transcript length, the ratio of modified bases per transcript correlates positively with ONT mRNA abundance but negatively with transcript length. Thus, shorter mRNAs tend to have a higher density of modified bases while expressed at higher levels.

Unexpectedly, we did not find evidence that the endogenous induction of oxidative stress is associated with increased RNA oxidation represented by 8-oxoGuo. Moreover, we found the lowest number of modified mRNA sites (n=1,220) when comparing atheroprotective VSMCs (C3) with oxidatively stressed VSMCs (C1) (**Suppl. Table S8**).

However, comparison of atheroprotective VSMCs (C3) and pro-atherogenic VSMCs (C4) yielded the largest number of detectable mRNA modification sites (2.1 million in C3 vs. C4), from which 5,989 high-confidence differentially modified RNA bases (DMRs) were identified after multiple-testing correction (FDR ≤ 0.05; **Suppl. Table S6** and **S7**). Subsequent filtering for a differential modification rate of at least 25% kept 2,186 differential sites. These DMRs most likely reflect multiple modification types affecting adenosine, cytidine, and uridine (**Suppl. Figure S5**) which appear to be cytokine-dependent rather than stress-induced.

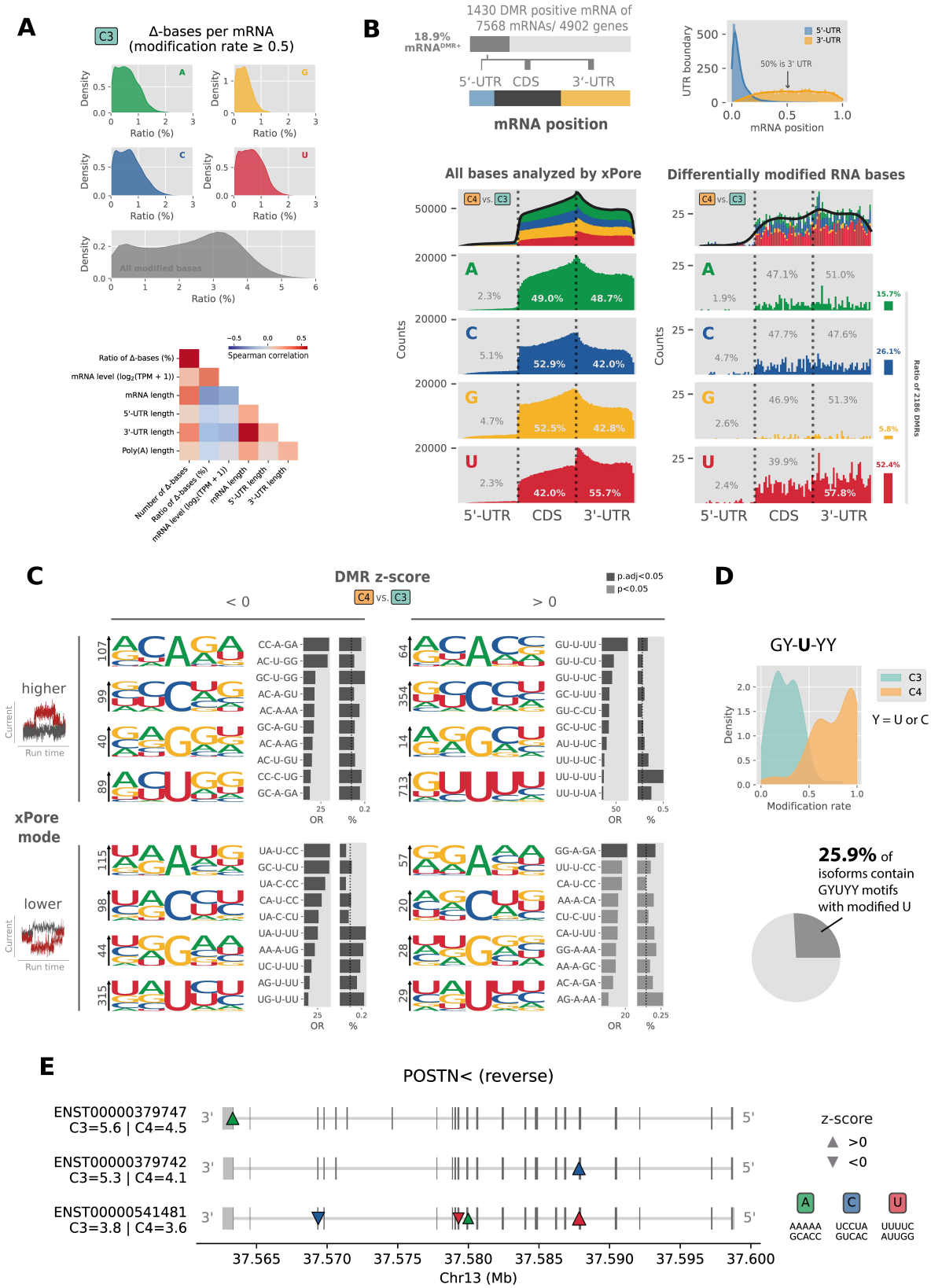

Figure 2: Detection of RNA base modifications by ONT direct RNA sequencing and xPore in vascular smooth muscle cells. VSMCs were treated with atheroprotective TGF-β1 (C3) or pro-inflammatory PDGF-BB / IL-1β (C4) (n=3 technical replicates). Approximately 4 million base positions across 7,568 transcripts were analyzed. (**A**) The proportion of modified (Δ) RNA bases (rate ≥ 0.5) in TGF-β1–treated VSMCs peaks at 2 to 4%. A Spearman correlation matrix is shown below. (**B**) A total of 2,186 significantly differentially modified RNA bases (DMRs)

were identified in UTRs and coding sequences (CDS) across 1,430 transcripts. The relative distribution of RNA bases (A, C, G, U) within UTRs and CDS is shown for all analyzed positions (left) and for significant DMRs (C4 vs. C3; right). (**C**) Sequence motif analysis highlights the GUUUU motif with higher modification rates of uridine in C4 (DMR z-score > 0). The xPore mode "higher" indicates increased Nanopore current at modified bases. The odds ratio (OR) and percentage (%) of the 10 most abundant sequence motifs (5-mers) are shown next to the motif plots. (**D**) Distribution of modification rates for the central uridine in GY–U–YY motifs (adjusted $p < 0.05$; rate ≥ 0.25), representing ~26% of all DMR-positive mRNAs. (**E**) *POSTN* transcripts illustrate isoform-specific DMRs.

We observed that PDGF-BB treatment led predominantely to enhanced modification of uridines in pro-athorogenic VSMCs (PDGF-BB / IL-1β; C4) as well as oxidatively stressed VSMCs (TGF-β1 > PDGF-BB / IL-1β > PDGF-BB boost; C1) (**Figure 2B-D** and **Suppl. Figure S6**). The highest number of modified uridines were found in highly energetic, metabolic active and cytokine-produncing VSMCs. Uridine modifications often occurred in GY-U-YY motifs, with Y being a pyrimidine base (C or U). Thereby, GUUUU was the most prevalent 5-mer context (209 DMR sites in 194 transcripts), showing ~80-fold enrichment across all mRNA sequences analyzed with xPore (**Figure 2C**). Affected genes appear to be regulated by the transcription factors TCF-21, JUN (c-Jun) or JunD and are enriched for epithelial-mesenchymal transition, immune system, cell migration, and the PI3K/AKT/mTOR signaling pathway (**Suppl. Table S9**). Analysis with xPore revealed that many transcripts harbor multiple differentially modified sites, and co-modification of uridine together with adenosine and/or cytidine was frequently observed (cf. **Suppl. Table S10**). Overall, the comparison of atheroprotective VSMCs (C3) and pro-atherogenic VSMCs (C4) yielded 1,258 genes expressing transcripts that contain one or more DMR-sites, with the top affected genes *FN1* (18 sites, 9 transcripts), *ITGB1* (15 sites, 12 transcripts), *HDLBP* (13 sites, 3 transcripts), and *TUBB* (10 sites, 5 transcripts) (cf. **Suppl. Table S11**). Of note, *FN1* and *ITGB1* are described to be major regulators of VSMCs.[34] Other DMR-affected genes and transcripts involved in VSMC-relevant processes are highlighted in **Suppl. Table S12** and **Suppl. Figure S7**. Except *COL6A2* and *PXDC1* (**Suppl. Figure S4B** and **S4C**), none of these notably DMR-affected genes is among the 272 genes for which significant differential splicing was detected between atheroprotective and pro-atherogenic VSMCs (**Suppl. Table S4**), suggesting that DMRs may not affect alternative splicing.

342

343 *Association of base modification with protein abundance*

344 Since we detected the largest number of DMRs when comparing atheroprotective (TGF-1β;
345 C3) with pro-atherogenic VMCs (PDGF-BB / IL1-β1; C4), we subsequently quantified the
346 proteome of these VSMCs phenotypes (**Suppl. Table S13**), resulting in 4,995 identified
347 proteins of which 1,171 were significantly differentially abundant after multiple testing
348 correction (**Suppl. Table S14**). Enrichment analysis confirms the pro-inflammatory signature
349 of PDGF-BB / IL1-β1-treated VSMCs (**Figure 3A**). In order to investigate a potential role of
350 RNA modifications on protein levels, we focused on transcripts detected at a minimum of 10
351 transcripts per million (TPM) in both Illumina and ONT sequencing. At this threshold,
352 log10-transformed RNA levels derived from Illumina and ONT correlate best, with a
353 Pearson's correlation coefficient of r=0.66 for C3 and r=0.67 for C4 (cf. **Suppl. Figure S8**),
354 which is within ranges reported previously[35]. In addition, transcript counts were aggregated
355 per gene since proteomics is not isoform-sensitive. Protein levels align with gene expression
356 levels in atheroprotective VSMCs (TGF-1β; C3) when only non-zero values are considered,
357 and this relationship is independent of the presence of differentially modified RNA bases
358 (DMRs in C4 vs. C3). However, DMRs are more frequently identified at higher gene/protein
359 levels (**Figure 3B**). Notably, the proportion of DMR-positive mRNAs decreases from
360 approximately 22% among mRNAs with detectable protein to about 8% among those for
361 which no corresponding protein was detected - despite comparable mRNA levels -
362 suggesting that some DMRs may be crucial for translation activity. Moreover, for genes
363 linked to more than three DMRs, changes in transcript abundance were strongly mirrored at
364 the protein level. This is reflected by a strong correlation between the $\log_2$ fold change in
365 gene expression and the corresponding $\log_2$ fold change in protein abundance. (**Figure 3C**).
366 This relationship supports a role for DMRs in shaping transcriptional programs that extend to
367 protein expression, particularly for genes linked to the TCF21-regulated atheroprotective,
368 fibroblast-/mesenchymal-like VSMC state (C3). A subset of these genes is downregulated

during the transition to the pro-inflammatory VSMC phenotype (C4). An overview of genes with notable differences in corresponding protein levels is shown in **Figure 3D**. Neither the relative position of DMRs within UTRs or coding sequences nor the direction of modification changes suggests a consistent rule governing DMR-dependent transcriptional or translational regulation. Nonetheless, we observe a trend toward reduced adenosine modification (z-score < 0) in genes exhibiting higher protein abundance in pro-atherogenic VMCs, and the opposite trend in genes with lower protein abundance. Moreover, cytidines appear to be differentially modified more frequently when located in the 5'-UTR of genes associated with increased protein levels.

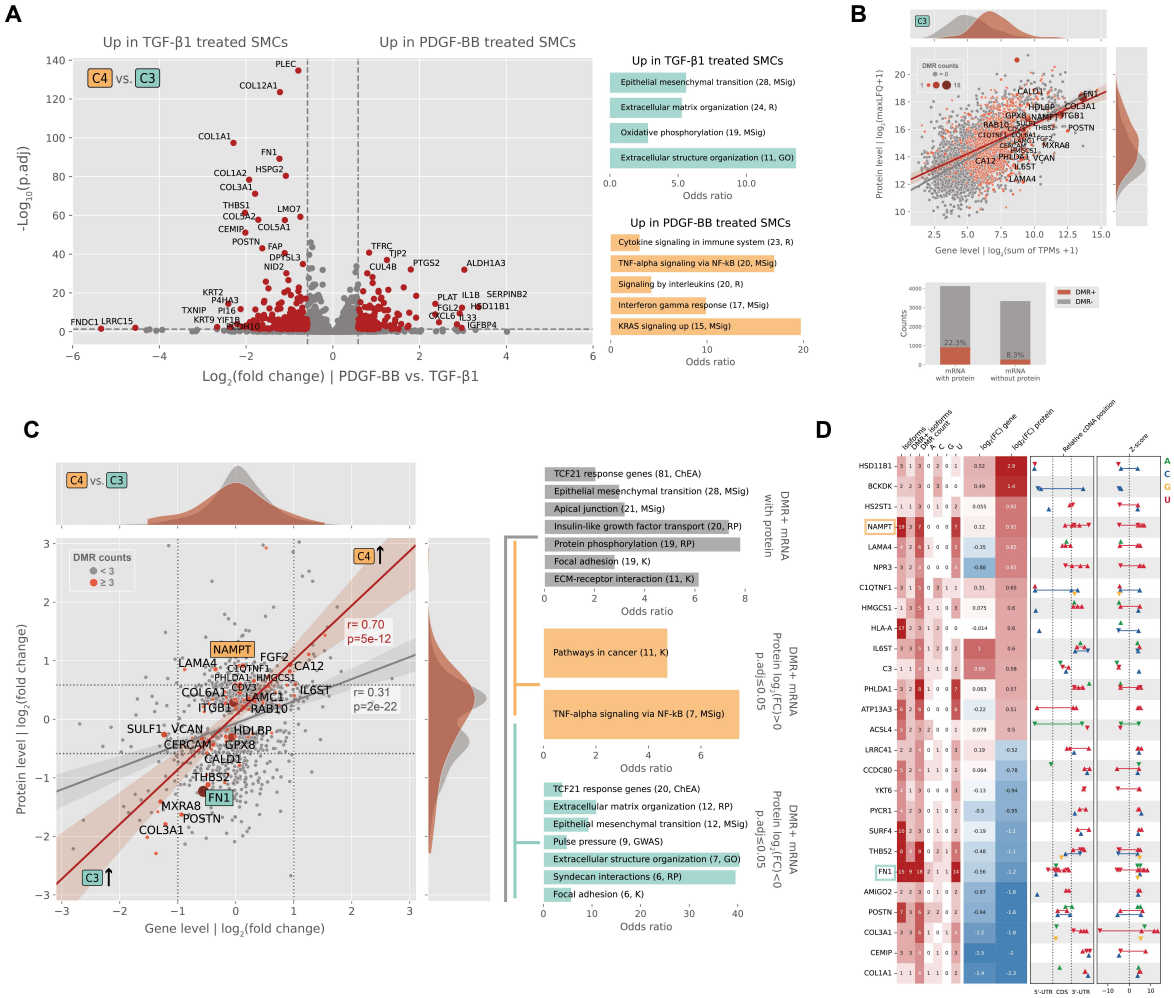

Figure 3: Impact of RNA base modifications on translational activity in smooth muscle cells. (**A**) Differential proteomic analysis of VSMCs treated with TGF-β1 (C3) or PDGF-BB / IL-1β (C4) (n = 4 technical replicates per condition). Volcano plot and enrichment analyses highlight canonical TGF-β1– and PDGF-associated proteins and pathways (GO=Gene Ontology; MSig=Molecular Signature database; R=Reactome database). (**B**) Regression analysis of gene-level versus protein-level expression in C3 for transcripts with (red) or without (gray)

differentially modified RNA bases (DMRs; C3 vs. C4). Point size reflects the number of DMRs per gene across all isoforms. (**C**) Same analysis as (**B**) using $\log_2$ fold changes (C3 vs. C4). The Pearson correlation (r; significance assessed with t-test) was calculated for genes with ≥ 3 DMRs across all isoforms and < 3 DMRs. Gene set enrichment analysis was performed for genes with ≥ 3 DMRs and stratified by corresponding protein $\log_2$ fold change (> 0 or < 0). (ChEA=ChIP-X enrichment analysis; GWAS= GWAS catalog; K; KEEG database; RP = Reactome Pathways). (**D**) Overview of genes with $|\log_2 FC| > 0.5$ (FC=fold change), discordant gene–protein $\log_2 FC$ (> 0.25), and > 2 DMRs across all isoforms; including isoform counts, DMR position in untranslated regions (UTR) or coding sequence (CDS), and z-scores (C4 vs. C3) with xPore mode as arrows ("higher"=up, "lower"=down).

Transcriptomic landscape of mRNA modification–related genes

Since uridine was the most frequently modified RNA base, we first examined the expression level of pseudouridine synthase genes in atheroprotective and pro-atherogenic VSMCs. We observed modest yet significant downregulation of three of them, but only in PDFG-treated, oxidatively stressed VSMCs (C1) (**Suppl. Figure S9**). In contrast, a notable increase in *PUS7* level was observed in pro-atherogenic VMCs, reaching nominal significance (p = 0.022, p.adj = 0.098) (**Figure 4A**). Among all mRNA modification–related genes (median $\log_2$ normalized counts > 5; cf. **Suppl. Table S15**), significant differences between atheroprotective and pro-atherogenic VSMCs were detected only for *TET1* (hm5C oxidase) after adjustment for multiple testing (p.adj. < 0.05). Although it appears that only a few mRNA modifiers and genes encoding for mRNA-binding proteins differ individually, the global expression signatures clearly separate the two VSMC phenotypes (**Suppl. Figure 4B**), suggesting an orchestrated program of mRNA modification–related genes that promote either atheroprotective or pro-atherogenic pathways.

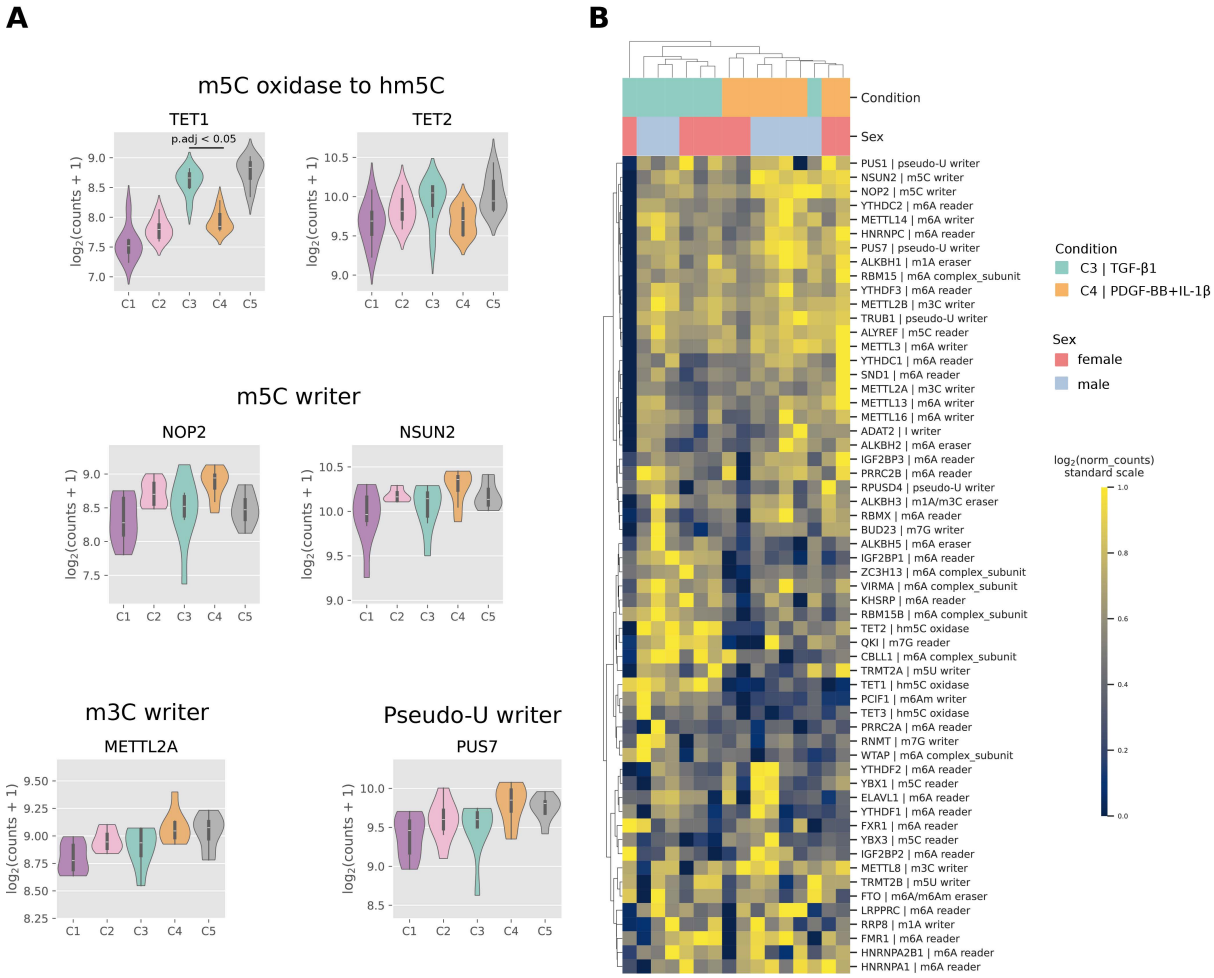

Figure 4: Expression pattern of genes encoding mRNA-modifying enzymes in atheroprotective (C3) and pro-atherogenic (C4) VSMCs. (**A**) Violin plots of genes whose canonical transcripts are differentially expressed in C3 vs. C4 at nominal significance ($p < 0.05$; for TET1: p.adj < 0.05; **Suppl. Table S3**). (**B**) The clustermap shows the standardized expression level of genes with median log2(normalized counts) ≥ 5 (**Suppl. Table S15**).

RNA base modifications influence poly(A) tail dynamics

Next, we examined how DMRs influence mRNA processing and translational regulation, including poly(A) tail dynamics. Density plots of poly(A) tail lengths in atheroprotective (TGF-1β; C3) and pro-atherogenic VMCs (PDGF-BB / IL1-β1; C4) reveal that genes/transcripts with increasing numbers of DMRs exhibit progressively longer poly(A) tails, along with more pronounced differences between the two VSMC phenotypes (**Figure 5A**). In addition, we observed a strong correlation between gene/protein $\log_2$ fold changes and corresponding shifts in poly(A) tail length. Longer poly(A) tails appear to be associated with lower mRNA levels as well as protein levels in pro-atherogenic VSMCs (**Figure 5B**). This relationship is highlighted for *NAMPT* and *FN1* in **Figure 5C,** which were the only ones with significant differences in poly(A) tail length after adjusting for multiple testing (cf. **Suppl. Table S16**). While *NAMPT* shows higher expression in pro-atherogenic VSMCs (C4), accompanied by shorter poly(A) tails, *FN1* exhibits the opposite pattern when all isoforms are considered. Interestingly, several uridines show increased modification rates (in “higher” xPore mode) in pro-atherogenic VSMCs. These modified uridines are located predominantly in the 3′-UTRs of *NAMPT* isoforms, whereas in *FN1* isoforms they occur exclusively within coding sequences.

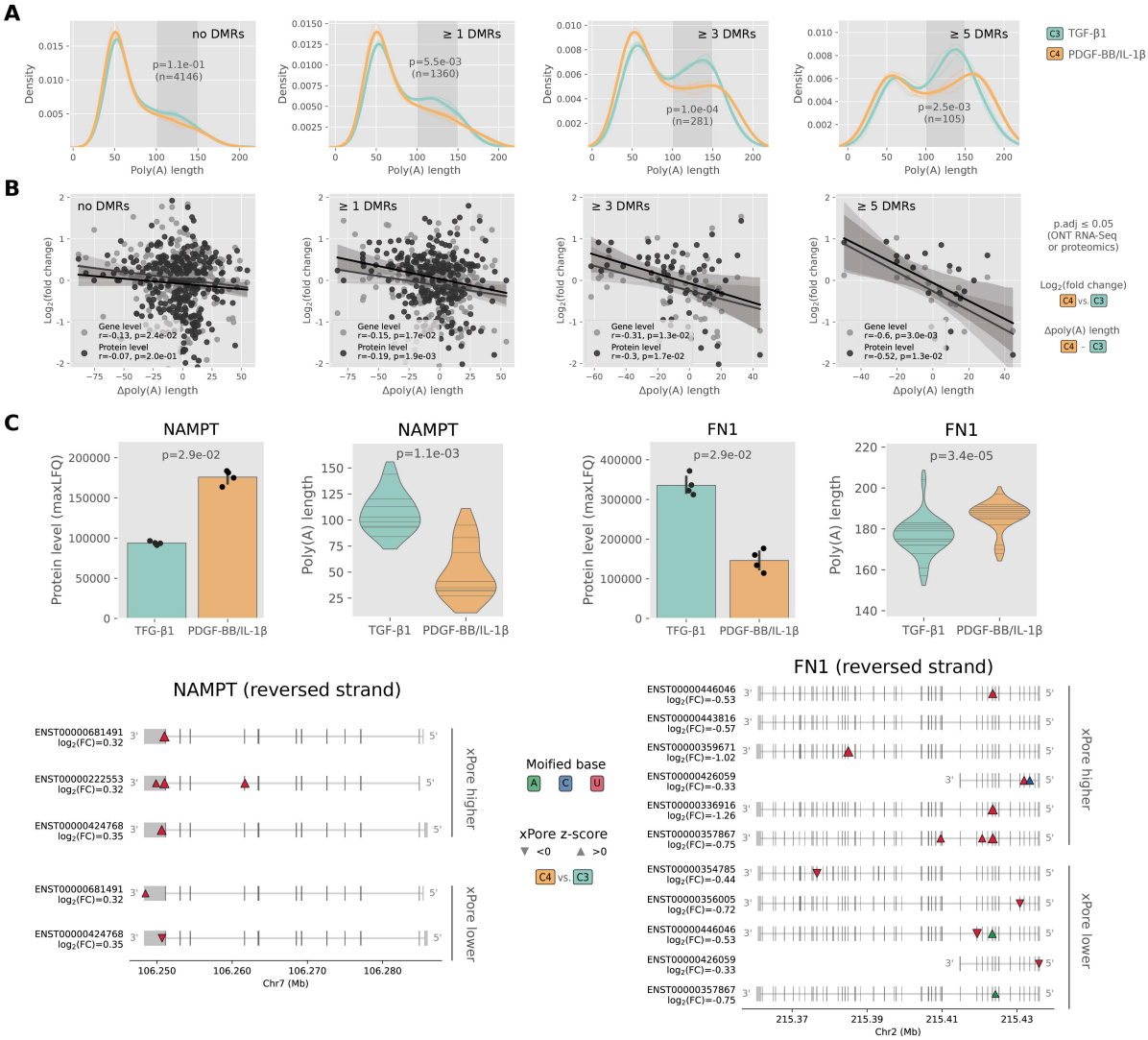

Figure 5: Poly(A) tail length distribution of mRNAs isolated from TGF-β1– (C3) or PDGF-BB / IL-1β–stimulated vascular smooth muscle cells (C4). (**A**) Kernel density plots show increasing poly(A) tail length and greater differences between C3 and C4 with increasing number of differentially modified RNA bases (DMRs). Statistical significance was calculated using a permutation test in the region 100 to 150 adenosines, with transcripts counts in parentheses. (**B**) Pearson correlation plots of difference (Δ) in poly(A) tail length versus $\log_2$ fold change for differentially expressed genes/proteins (p.adj ≤ 0.5). Significance assessed with t-test. (**C**) Examples illustrating the relationship between protein abundance (n=4 technical replicates), poly(A) tail length, and DMR position (n=3 technical replicates). Poly(A) tail lengths across all isoforms (polya coverage > 10; FN1 = 9 isoforms, NAPT = 3) and technical replicates (n=3) are shown per gene; significance was assessed by Mann–Whitney U tests. Lower panels display isoforms with DMRs stratified by xPore mode ("higher" or "lower"), with $\log_2$ fold change (C4 vs. C3) shown for each transcript.

Modified uridine bases are enriched in accessible RNA secondary structures in the 3'-UTR

Next, we predicted RNA secondary structures of 150-nucleotide sequences containing DMR sites using the ViennaRNA library to investigate whether DMRs might be found more frequently in distinct structural elements. In brief, 65 controid RNA secondary structures were predicted per transcript and DMR position by shifting a 150 nucleotide window two

bases downstream, starting from 140 nucleotides upstream of the DMR position. Centroid RNA secondary structures were clustered based on similarity scores. The RNA secondary structure with the lowest MFE of the most representative cluster (selected upon cluster size, median MFE, and MFE variance) was taken for over-representation analysis (**Figure 6A**). As part of our quality control, we examined the negative minimal free energy (MFE) of all predicted centroid RNA secondary structures across relative cDNA positions. Consistent with previous observations, the negative median MFE per position declines toward the 3′-UTR, accompanied by reduced GC content, a hallmark of functional mRNAs[36] (**Figure 6B**). Over-representation analysis of DMRs in RNA secondary structure elements revealed that differentially modified uridines are 1.7-fold enriched in interior loops in 3'-UTRs (**Figure 6C** and **Suppl. Table S17**).

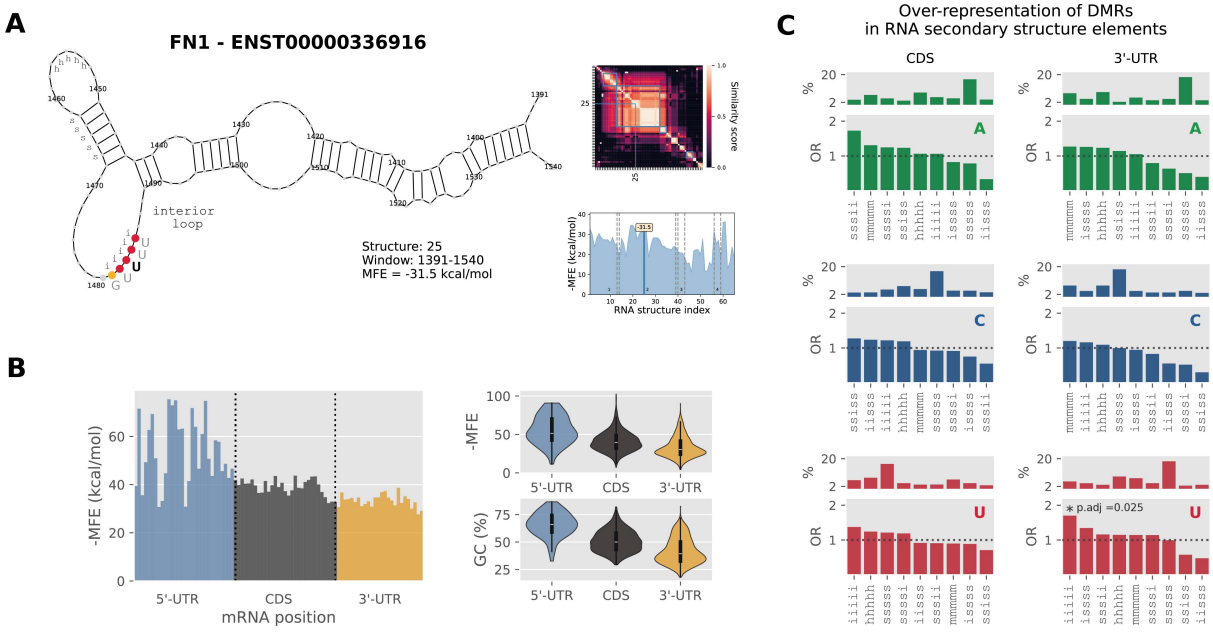

Figure 6: Distribution of differentially modified RNA bases in secondary RNA structures. (**A**) RNA secondary structures surrounding DMRs were predicted from sliding 150-nt windows using the ViennaRNA package. Centroid structures with minimal free energy (MFE) were clustered, and dominant secondary structure elements (5-mers) were extracted. (**B**) Mean MFE per binned relative DMR positions (90 bins) in 5′/3′-UTR (untranslated region) and coding sequence (CDS). Violin plots highlight the correlation of MFE and GC-content. (**C**) Differentially modified uridines are enriched in predicted interior loops (iiiii) within 3'-UTR (Fisher's exact test). Bar plots show relative abundance (%) and odds ratios (OR) of secondary structure elements across 343 A, 571 C and 1,146 U DMRs (*cf.* **Suppl. Table S17**).

Modified RNA bases may modulate miRNA binding

Moreover, we detected an excess of modifications near stop codons at the beginning of the 3'-UTR (*cf.* **Figure 2B**), which has also been reported previously by the authors of xPore[8]. We hypothesize that this enrichment is related to DMRs that influence miRNA binding, as miRNA-to-mRNA binding is reported to be most effective when occurring at the beginning or the end of long 3′-UTRs.[37] Therefore, we assessed the potential impact of DMRs on miRNA binding. We quantified miRNA expression in four VSMC states (C2 to C5) and screened highly expressed miRNAs ($\log_2$(count) ≥ 10 in one replicate) for miRNA-binding sites based on direct 8-mer seed matches. We identified 60 of the 202 highly expressed miRNAs whose seed sequences could directly bind to DMR-containing mRNA regions in 3'-UTR (**Figure 7A** and **Suppl. Table S18**).

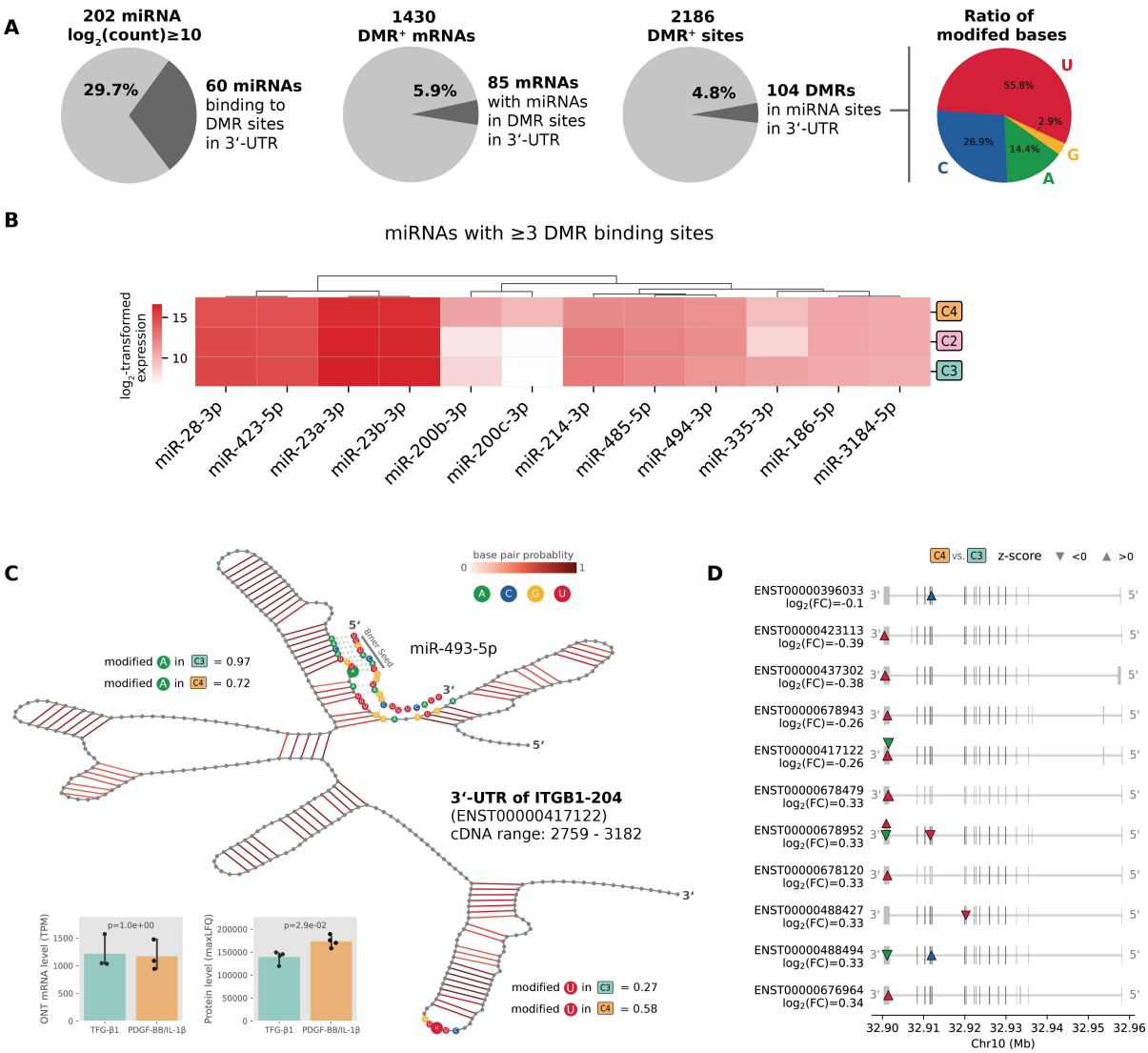

Figure 7: Potential binding of miRNAs at differentially modified RNA bases (DMRs). (**A**) Pie charts summarize highly expressed miRNAs ($\log_2$ count ≥ 10) predicted to bind DMRs via 8-mer seed sequences, the fraction of DMR-positive transcripts and DMRs within 3′ UTR miRNA binding sites, and the proportion of modified bases at these sites. (**B**) Expression pattern of highly expressed miRNAs with more than three predicted DMR binding sites across three conditions (C2=TGF-β1 > PDGF-BB / IL-1β, C3=TGF-β1, C4=PDGF-BB / IL-1β). (**C**) *ITGB1* isoform ITGB1-204 illustrates a modified adenosine within a validated miR-493-5p binding site[38], showing reduced modification in PDGF-BB / IL-1β–treated cells accompanied by increased ITGB1 protein levels. A second DMR was identified downstream, with enhanced uridine modification in C4. (**D**) Overview of DMRs across ITGB1 isoforms, with $\log_2$ fold change (FC; C4 vs. C3) shown below each Ensembl transcript. Triangles indicate increased or decreased modification.

498 The highest number of DMR binding sites was detected for miR-494-3p (n = 6), followed by
499 miR-186-5p, miR-200b/c-3p, and miR-28-3p (n = 4) (**Figure 7B**). DMR-miRNA pairs were
500 found for 85 mRNAs and 104 DMRs, thereby affecting about 6% of all DMR-positive
501 transcripts. Of those, 58 sites have uridine modified, 28 cytidine, 15 adenosine, and 3
502 guanosine (**Figure 7A**). However, miRNA binding for only six genes had experimental
503 evidence and a respective publication recorded in the miRTarBase database. In addition, the
504 specific binding site of miR-493-5p at the unique DMR-site AA-A-UG of *ITGB1-204* in
505 3'-UTR (cDNA position 2859) was the only one experimentally confirmed[38], but not yet
506 recorded in miRTarBase. **Figure 7C** illustrates a possible miRNA binding model postulating
507 that miR-493-5p directly binds to a modified adenosine located in the AA-A-UG sequence.
508 Another DMR site (GU-U-UC) is located about 230 nucleotides downstream at the tip of a
509 hairpin loop. Interestingly, the mRNA levels are similar in atheroprotective (TGF-1β; C3) and
510 pro-atherogenic VMCs (PDGF-BB / IL1-β1; C4), yet integrin β1 protein levels appear to be
511 higher in the latter VMC phenotype. In this model, elevated uridine modification in
512 pro-atherogenic VMCs, particularly within a hairpin loop, could promote mRNA stability or
513 reinforce RNA structural integrity. Conversely, decreased adenosine modification may
514 reduce miRNA-binding efficiency, thereby limiting miRNA-mediated translational repression.
515 Notably, the miRNA context-binding sequence is conserved across all *ITGB1* isoforms,
516 where modified uridines or adenosines lie nearby (**Figure 7D**).
517 In order to investigate whether increased levels of miRNAs can influence RNA base
518 modification, *e.g.*, by decorating the modifiable site, we profiled the mirNOME in phenotypic
519 transition conditions C2 to C5 (**Suppl. Table S19** and **S20**). In total, 131 miRNAs were
520 significantly differentially expressed across all four conditions, with the top four being
521 miR-145-5p, miR-204-5p, miR-146a-5p, and miR-5585-3p. Thereby, miR-145-5p showed
522 the greatest expression difference, exhibiting a ~4-fold higher abundance in TGF-β1–treated
523 VSMCs (C3) compared with PDGF-BB / IL-1β–treated VSMCs (C4) (**Suppl. Table S20**).
524 This is consistent with prior studies demonstrating time- and dose-dependent

525 downregulation of miR-145-5p under PDGF stimulation.[39] However, neither for miR-145-5p
526 nor the other differentially expressed mRNAs did we find evidence that miRNA binding
527 directly affects RNA base modifications at specific miRNA binding sites.
528

529 **Discussion**

530 Using Nanopore direct RNA-Seq, we performed a transcriptome-wide, untargeted screening
531 of RNA base modifications in vascular smooth muscle cells (VSMCs) under atheroprotective
532 (TGF-β1) and pro-atherogenic (PDGF-BB / IL-1β) treatment. Our main findings are that 1)
533 up to 5% of mRNA bases appear to be modified (*e.g.*, methylated). 2) Differences in mRNA
534 base modifications between atheroprotective and atherogenic VSMC phenotypes often
535 occur near stop codons and at the beginning of 3'-UTRs, specifically affecting uridines in
536 accessible 3'-UTR regions. 3) The G-Y-U-YY (with Y=U/C) is the most prominent motif found
537 in ~26% of isoforms. 4) Differentially modified RNA bases might be explained by global
538 changes in RNA-modifying enzyme levels. 5) DMRs might be linked to translation activity,
539 *e.g.,* by regulating Poly(A) tail dynamics and miRNA binding.
540 These findings expand the understanding of VSMC phenotype switching in the context of
541 atherosclerosis beyond transcriptional and epigenetic regulation.[5] Although we were not able
542 to detect traces of mRNA oxidation in oxidatively stressed VSMCs using Nanopore direct
543 RNA-Seq, our multi-level analysis suggests that mRNAs can harbor multiple types of base
544 modifications. Further, pro-inflammatory cytokines can influence the epitranscriptomic
545 landscape by altering the expression levels of RNA-modifying enzymes. For example,
546 nominally significant shifts in mRNA abundance for the pseudouridine writer *PUS7* and
547 several m^5C modifiers (*TET1*, *TET2*, *NOP2*, *NSUN2*) may explain the higher rate of uridine
548 and cytidine modification in pro-atherogenic VMCs detected by xPore. However, the
549 molecular mechanisms and temporal dynamics underlying cytokine-induced regulatory
550 programs that involve several classes of mRNA-modifying enzymes are largely unresolved.
551 In particular, the signaling pathways and transcription factors that control the expression of

552 specific mRNA-modifying enzymes, the stability of these enzymes under defined conditions,
553 and the kinetics of base modification on endogenous mRNAs remain to be elucidated.
554 The most strongly enriched sequence context was the GY-U-YY motif (Y = pyrimidine base,
555 C or U). To our knowledge, this motif has not been described so far. Our
556 epitranscriptome-wide analyses suggest that modification of uridine may foster the
557 PI3K/AKT signaling pathway triggered by PDGF stimulation[40] by stabilizing transcripts
558 essential for this pathway while destabilizing transcripts associated with antagonistic
559 pathways. For example, many uridine-modified transcripts downregulated in pro-atherogenic
560 VSMCs are under the control of the transcription factor TCF21, which normally suppresses
561 PI3K/AKT signaling.[41] TCF21 is known as a key driver of VSMC state transitions in
562 atherosclerosis[2,] and the fact that many base-modified transcripts are regulated by TCF21
563 highlights the importance of mRNA base modifications in atherosclerosis.
564 To elucidate regulatory mechanisms underlying differentially modified RNA bases (DMRs),
565 we investigated multiple possible consequences of DMRs on mRNA processing. We
566 analyzed the impact of DMRs on mRNA splicing but did not find evidence for
567 pathway-relevant differences in isoform usage in a DMR-dependent manner. In fact, DMRs
568 were often found in proximity to stop codons in agreement with previous studies[8,42],
569 indicating rather regulatory activity that might impact mRNA usage, mRNA folding, mRNA
570 stability, or miRNA binding, and thus translational output.
571 First, we observed a negative correlation of protein abundance and poly(A) tail lengths,
572 particularly for transcripts harboring DMRs, which is in line with a previous study that also
573 applied Nanopore direct RNA-Seq[42]. The potential contribution of DMRs highlights, indeed,
574 the regulatory potential of these modifications.
575 Second, uridine modifications were enriched in predicted single-stranded RNA structure
576 elements in 3'-UTRs, supporting the regulatory nature of these mRNA modifications, as
577 these regions are potentially accessible for RNA-modifying enzymes and allow binding of
578 proteins that exert post-transcriptional regulatory effects. The vast majority of significantly

579 differential modifications affected uridine, likely representing pseudouridine (Ψ), which is the
580 most common RNA modification. For Ψ, both stabilizing and destabilizing effects on mRNA
581 were described[43], and the examples of *NAMPT* and *FN1* hint that uridine modification in
582 3'-UTRs might be associated with enhanced mRNA stability and increased translational
583 output (*cf. NAMPT*), whereas uridine modification within coding sequence could potentially
584 have opposite consequences (*cf. FN1*).

585 Third, it has been demonstrated that mRNA modifications can modulate miRNA binding
586 when located in seed match regions in 3′-UTR miRNA binding sites.[44] Notably, 60 out of 202
587 highly expressed miRNAs could directly bind to DMRs with their seed sequence, and
588 modified uridine accounts for ~56% of all affected DMR-sites. Although none of the
589 predicted uridine modification-related miRNA binding sites were experimentally validated
590 according to miRTarBase, we hypothesize that some of the identified uridine modifications in
591 3′-UTR can weaken miRNA binding and thereby prolong mRNA half-life and promote
592 translational output. Nonetheless, additional in-depth studies are required to elucidate the
593 regulatory implications of uridine modifications. Since some of the DMR-related miRNAs are
594 directly related to SMC biology and atherosclerosis (*e.g.*, miR-22, miR-143, miR-145,
595 miR-200, miR-424)[45,46], the notion of mRNA modifications affecting miRNA regulation might
596 help to optimize miRNAs as novel therapeutics.

597 While this study is the first one that comprehensively combines investigations based on
598 short-read sequencing, long-read direct RNA sequencing, as well as mass spectrometry,
599 such multi-platform integration has technical limitations. For example, there is still a
600 discrepancy between short-read RNA-Seq and long-read RNA-Seq with respect to
601 determining expression estimates[47], as well as mapping of reads. Further, quantification of
602 long reads can be affected by incomplete transcript references, and recently, a large number
603 of novel transcripts have been detected in a similar experimental setup to ours[19]. Despite the
604 higher mapping accuracy of long-read sequencing, the limited throughput of MinION flow
605 cells restricted ONT analyses to highly expressed genes that exhibit similar expression

levels in two conditions, preventing differential modification testing for many transcripts. Consequently, insufficient coverage and limited replicates likely led to a considerable proportion of missed DMRs, which may explain the low number of detected modifications in oxidatively stressed VSMCs despite differential expression of multiple genes related to mRNA modification. Moreover, the time point of DMR assessment after cytokine stimulation might be crucial, as some RNA base modifications might lead to rapid mRNA degradation.

A further challenge in assessing the regulatory impact of DMRs on translational output is that the protein quantification relied on peptide-based measurements, which generally permit assignment at the gene level but not at the transcript level, thereby limiting the linkage of isoform-resolved DMRs to protein expression.

Another limitation is the use of the modification-type agnostic detection approach. Although k-mer context and enzyme-related gene expression can suggest specific modification types (e.g., the DRACH motif for m6A), we did not detect strong signals of known sequence motifs at differential sites. Moreover, the ONT RNA002 chemistry precluded the use of ONT basecalling models for specific modifications, which are currently available only for RNA004 chemistry[48] (*cf.* https://genesilico.pl/modomics/tools). Consequently, accurate classification of individual, specific modification types will require dedicated technologies and experimental validation in future studies.

In conclusion, our modification-type-agnostic approach provides a comprehensive, transcriptome-wide view of the RNA modification landscape underlying VSMC phenotypic transitions. We show that distinct RNA modification types frequently co-localize within the same transcripts, particularly near stop codons, suggesting combinatorial regulatory effects on processes such as polyadenylation, mRNA stability, and interactions with regulatory proteins or miRNAs. Moreover, our data indicate that mRNA base modifications – especially uridine modifications – act as post-transcriptional regulators that fine-tune cytokine-induced, transcription factor–specific signaling pathways and help maintain atherosclerosis-relevant SMC phenotypes. Finally, modification sites may serve as targets for miRNA-based

633 therapeutic strategies, and base modifications may be detectable in circulating cell-free
634 RNA, highlighting their potential as biomarkers of disease severity.
635

636 **Acknowledgments**
637 Initial investigations of the ONT data and of xPore results were performed by Lalitha
638 Kamada as part of her Master's thesis, which was co-supervised by IW and Sven Rahmann
639 and conducted within the Medical Systems Biology Group of Hauke Busch. We are further
640 grateful to Jeanette Erdmann (deceased 2023), former head of the Institute on
641 Cardiogenetics at the University of Lübeck, for supporting the research environment in which
642 this work was conducted. This work used the high-performance computing infrastructure at
643 the Research Center Borstel, Leibniz Lung Center.
644

645 **Sources of Funding**
646 This work was supported by a miniproposal from the Cluster of Excellence Precision
647 Medicine in Chronic Inflammation to T.R. and I.W.; Deutsche Forschungsgemeinschaft
648 [grant numbers 407495230, 423957469 to J.F.] and the German Centre for Cardiovascular
649 Research [grant number 81Z0700107 to T.Z.]. T.Z. is co-inventor of an international patent
650 on the use of a computing device to estimate the probability of myocardial infarction
651 (International Publication No. WO2022043229A1) and is a shareholder in ART.EMIS GmbH
652 Hamburg.
653

654 **Disclosures:** The authors declare that they have no conflict of interest.
655

656 **Supplemental Material**
657 - Supplementary Methods (PDF)
658 - Supplementary Figures S1-S9 (PDF)
659 - Supplementary Tables S1-S20 (XLSX)

References

1. Sarraju, A. & Nissen, S. E. Atherosclerotic plaque stabilization and regression: a review of clinical evidence. *Nat Rev Cardiol* **21**, 487–497 (2024).
2. Chen, R., McVey, D. G., Shen, D., Huang, X. & Ye, S. Phenotypic Switching of Vascular Smooth Muscle Cells in Atherosclerosis. *Journal of the American Heart Association* **12**, e031121 (2023).
3. Yap, C., Mieremet, A., de Vries, C. J. M., Micha, D. & de Waard, V. Six Shades of Vascular Smooth Muscle Cells Illuminated by KLF4 (Krüppel-Like Factor 4). *ATVB* https://doi.org/10.1161/ATVBAHA.121.316600 (2021) doi:10.1161/ATVBAHA.121.316600.
4. Grootaert, M. O. J. & Bennett, M. R. Vascular smooth muscle cells in atherosclerosis: time for a re-assessment. *Cardiovasc Res* **117**, 2326–2339 (2021).
5. Zurek, M., Aavik, E., Mallick, R. & Ylä-Herttuala, S. Epigenetic Regulation of Vascular Smooth Muscle Cell Phenotype Switching in Atherosclerotic Artery Remodeling: A Mini-Review. *Frontiers in Genetics* **12**, 1449 (2021).
6. Huang, J. & Fu, Y. Epigenetic leash on the epitranscriptome: unveiling a novel regulatory axis in vascular smooth muscle contractility. *Cardiovasc Res* **121**, 1803–1805 (2025).
7. Zhang, Y., Lu, L. & Li, X. Detection technologies for RNA modifications. *Exp Mol Med* **54**, 1601–1616 (2022).
8. Pratanwanich, P. N. *et al.* Identification of differential RNA modifications from nanopore direct RNA sequencing with xPore. *Nat Biotechnol* 1–9 (2021) doi:10.1038/s41587-021-00949-w.
9. Jonkhout, N. *et al.* The RNA modification landscape in human disease. *RNA* **23**, 1754–1769 (2017).
10. Nossent, A. Y. The epitranscriptome: RNA modifications in vascular remodelling. *Atherosclerosis* **374**, 24–33 (2023).
11. Stopa, V. *et al.* Epitranscriptomics in atherosclerosis: Unraveling RNA modifications, editing and splicing and their implications in vascular disease. *Vascul Pharmacol* **159**, 107496 (2025).
12. Fei, J., Cui, X.-B., Wang, J.-N., Dong, K. & Chen, S.-Y. ADAR1-Mediated RNA Editing, A Novel Mechanism Controlling Phenotypic Modulation of Vascular Smooth Muscle Cells. *Circ Res* **119**, 463–469 (2016).
13. Ye, W. *et al.* YY1 regulates vascular resistance and blood pressure dynamics through epigenetic control of m6A RNA modifications in vascular smooth muscle cells. *Cardiovasc Res* **121**, 1898–1916 (2025).
14. Zhao, Y. *et al.* METTL3-Mediated m6A mRNA Modification Facilitates Neointimal Hyperplasia in Arteriovenous Fistula. *Arteriosclerosis, Thrombosis, and Vascular Biology* **45**, 1124–1144 (2025).
15. Poulsen, H. E. *et al.* RNA modifications by oxidation: A novel disease mechanism? *Free Radical Biology and Medicine* **52**, 1353–1361 (2012).
16. Li, Y. & Wang, X. The role of DNA and RNA guanosine oxidation in cardiovascular diseases. *Pharmacological Research* **204**, 107187 (2024).
17. Guan, X. *et al.* Stress, Vascular Smooth Muscle Cell Phenotype and Atherosclerosis: Novel Insight into Smooth Muscle Cell Phenotypic Transition in Atherosclerosis. *Curr Atheroscler Rep* **26**, 411–425 (2024).
18. Camaré, C., Pucelle, M., Nègre-Salvayre, A. & Salvayre, R. Angiogenesis in the atherosclerotic plaque. *Redox Biol* **12**, 18–34 (2017).
19. Wu, H. *et al.* Nanopore long-read RNA sequencing reveals functional alternative splicing variants in human vascular smooth muscle cells. *Commun Biol* **6**, 1104 (2023).
20. Chen, C.-N. *et al.* Synergistic roles of platelet-derived growth factor-BB and interleukin-1beta in phenotypic modulation of human aortic smooth muscle cells. *Proc Natl Acad Sci U S A* **103**, 2665–2670 (2006).
21. Gleeson, J. *et al.* Accurate expression quantification from nanopore direct RNA

sequencing with NanoCount. *Nucleic Acids Res* **50**, e19 (2022).
22. Li, H. Minimap2: pairwise alignment for nucleotide sequences. *Bioinformatics* **34**, 3094–3100 (2018).
23. Love, M. I., Huber, W. & Anders, S. Moderated estimation of fold change and dispersion for RNA-seq data with DESeq2. *Genome Biol* **15**, 550 (2014).
24. Lewis, B. P., Burge, C. B. & Bartel, D. P. Conserved seed pairing, often flanked by adenosines, indicates that thousands of human genes are microRNA targets. *Cell* **120**, 15–20 (2005).
25. Cui, S. *et al.* miRTarBase 2025: updates to the collection of experimentally validated microRNA-target interactions. *Nucleic Acids Res* **53**, D147–D156 (2025).
26. Xie, Z. *et al.* Gene Set Knowledge Discovery with Enrichr. *Curr Protoc* **1**, e90 (2021).
27. Low, E. L., Baker, A. H. & Bradshaw, A. C. TGFβ, smooth muscle cells and coronary artery disease: a review. *Cell Signal* **53**, 90–101 (2019).
28. Pan, H. *et al.* Atherosclerosis Is a Smooth Muscle Cell–Driven Tumor-Like Disease. *Circulation* **149**, 1885–1898 (2024).
29. Ma, L. *et al.* IL-17 as a therapeutic target in cardiovascular diseases: Mechanistic insights and translational opportunities. *Pharmacological Research* **219**, 107879 (2025).
30. Farahzadi, R. *et al.* Oxidative stress regulation and related metabolic pathways in epithelial–mesenchymal transition of breast cancer stem cells. *Stem Cell Res Ther* **14**, 342 (2023).
31. Pang, S. *et al.* Correlation between the Serum Platelet-Derived Growth Factor, Angiopoietin-1, and Severity of Coronary Heart Disease. *Cardiology Research and Practice* **2020**, 3602608 (2020).
32. Lu, Q.-B. *et al.* Chicoric acid prevents PDGF-BB-induced VSMC dedifferentiation, proliferation and migration by suppressing ROS/NFκB/mTOR/P70S6K signaling cascade. *Redox Biology* **14**, 656–668 (2018).
33. Kalbe, B. *et al.* Olfactory Receptors Modulate Physiological Processes in Human Airway Smooth Muscle Cells. *Front. Physiol.* **7**, (2016).
34. Feil, S. *et al.* Smooth Muscle Cell-Derived Fibronectin Promotes an Atheroprotective Smooth Muscle Cell Phenotype Associated With Altered NO-cGMP Signaling. *J Am Heart Assoc* **14**, e040395 (2025).
35. Mock, A., Braun, M., Scholl, C., Fröhling, S. & Erkut, C. Transcriptome profiling for precision cancer medicine using shallow nanopore cDNA sequencing. *Sci Rep* **13**, 2378 (2023).
36. Palazzo, A. F. & Kang, Y. M. GC-content biases in protein-coding genes act as an “mRNA identity” feature for nuclear export. *BioEssays* **43**, 2000197 (2021).
37. Grimson, A. *et al.* MicroRNA targeting specificity in mammals: determinants beyond seed pairing. *Mol Cell* **27**, 91–105 (2007).
38. Liang, Z. *et al.* High expression of miR-493-5p positively correlates with clinical prognosis of non small cell lung cancer by targeting oncogene ITGB1. *Oncotarget* **8**, 47389–47399 (2017).
39. Li, L., Mao, D., Li, C. & Li, M. miR-145-5p Inhibits Vascular Smooth Muscle Cells (VSMCs) Proliferation and Migration by Dysregulating the Transforming Growth Factor-β Signaling Cascade. *Med Sci Monit* **24**, 4894–4904 (2018).
40. Xiao, Y. *et al.* PDGF Promotes the Warburg Effect in Pulmonary Arterial Smooth Muscle Cells via Activation of the PI3K/AKT/mTOR/HIF-1α Signaling Pathway. *Cellular Physiology and Biochemistry* **42**, 1603–1613 (2017).
41. Dai, Y. *et al.* TCF21 functions as a tumor suppressor in colorectal cancer through inactivation of PI3K/AKT signaling. *Onco Targets Ther* **10**, 1603–1611 (2017).
42. Kim, Y. *et al.* Nanopore direct RNA sequencing of human transcriptomes reveals the complexity of mRNA modifications and crosstalk between regulatory features. *Cell Genom* **5**, 100872 (2025).
43. Boo, S. H. & Kim, Y. K. The emerging role of RNA modifications in the regulation of mRNA stability. *Exp Mol Med* **52**, 400–408 (2020).

44. Lockhart, J., Canfield, J., Mong, E. F., VanWye, J. & Totary-Jain, H. Nucleotide Modification Alters MicroRNA-Dependent Silencing of MicroRNA Switches. *Mol Ther Nucleic Acids* **14**, 339–350 (2019).
45. Letonja, J. & Petrovič, D. A Review of MicroRNAs and lncRNAs in Atherosclerosis as Well as Some Major Inflammatory Conditions Affecting Atherosclerosis. *Biomedicines* **12**, 1322 (2024).
46. Lu, Y., Thavarajah, T., Gu, W., Cai, J. & Xu, Q. Impact of miRNA in Atherosclerosis. *Arteriosclerosis, Thrombosis, and Vascular Biology* **38**, e159–e170 (2018).
47. Pardo-Palacios, F. J. *et al.* Systematic assessment of long-read RNA-seq methods for transcript identification and quantification. *Nat Methods* **21**, 1349–1363 (2024).
48. Cappannini, A. *et al.* MODOMICS: a database of RNA modifications and related information. 2023 update. *Nucleic Acids Res* **52**, D239–D244 (2024).